Remote Sensing of Seasonal Climatic Constraints on Leaf Phenology Across Pantropical Evergreen Forest Biome

Qian Li, Xiuzhi Chen, Wenping Yuan, Haibo Lu, Ruoque Shen, Shengbiao Wu, Fanxi Gong, Yuhang Dai, Liyang Liu, Qingling Sun, et al.

AGU ADVANCING EARTH AND SPACE SCIENCE

Earth's Future

RESEARCH ARTICLE
10.1029/2021EF002160

Remote Sensing of Seasonal Climatic Constraints on Leaf Phenology Across Pantropical Evergreen Forest Biome

Qian Li[1], Xiuzhi Chen[1], Wenping Yuan[1], Haibo Lu[1], Ruoque Shen[1], Shengbiao Wu[2], Fanxi Gong[1], Yuhang Dai[1], Liyang Liu[3,4], Qingling Sun[1], Chaoqun Zhang[1,4], and Yongxian Su[4]

[1]Guangdong Province Key Laboratory for Climate Change and Natural Disaster Studies, School of Atmospheric Sciences, Sun Yat-sen University & Southern Marine Science and Engineering Guangdong Laboratory (Zhuhai), Zhuhai, China, [2]School of Biological Sciences, The University of Hong Kong, Hong Kong, China, [3]Laboratoire des Sciences du Climat et de l'Environnement, IPSL, CEA-CNRS-UVSQ, Université Paris-Saclay, Gif sur Yvette, France, [4]Key Lab of Guangdong for Utilization of Remote Sensing and Geographical Information System, Guangdong Open Laboratory of Geospatial Information Technology and Application, Guangzhou Institute of Geography, Guangdong Academy of Sciences, Guangzhou, China

Key Points:

- Sunlight dominantly controls whole seasonal leaf phenology across the pantropical region
- Atmospheric dryness is the main type of water stress for leaf phenology during the first half year
- Soil water stress is one main type of water stress in the first half year in tropical Asia and the second half of year in Congo

Supporting Information:

Supporting Information may be found in the online version of this article.

Correspondence to:

X. Chen,
chenxzh73@mail.sysu.edu.cn

Citation:

Li, Q., Chen, X., Yuan, W., Lu, H., Shen, R., Wu, S., et al. (2021). Remote sensing of seasonal climatic constraints on leaf phenology across pantropical evergreen forest biome. *Earth's Future*, *9*, e2021EF002160. https://doi.org/10.1029/2021EF002160

Received 23 APR 2021
Accepted 13 AUG 2021

Author Contributions:

Conceptualization: Xiuzhi Chen
Data curation: Qian Li
Methodology: Qian Li, Xiuzhi Chen
Software: Qian Li
Writing – original draft: Qian Li
Writing – review & editing: Xiuzhi Chen, Wenping Yuan, Haibo Lu, Ruoque Shen, Shengbiao Wu, Fanxi Gong, Yuhang Dai, Liyang Liu, Qingling Sun, Chaoqun Zhang, Yongxian Su

Abstract Climatic drivers for canopy leaf shedding and flush of evergreen broadleaved forest biome are still unclear at the continental scale across tropical and subtropical region. This imposes a challenge for modeling pantropical photosynthesis seasonality in Earth system models. Here, we examined three potential climatic triggers, vapor pressure deficit–a proxy of atmospheric water deficit, downward shortwave incoming solar radiation–a proxy of sunlight availability, and terrestrial water storage–a proxy of soil water availability observed by the Gravity Recovery and Climate Experiment, by comparing with two satellite phenological proxies–the Enhanced Vegetation Index and Continuous Solar-induced chlorophyll fluorescence. Results show that tropical leaf phenology varies greatly from equatorial bimodal seasonality to higher-latitude unimodal seasonality. Sunlight availability dominantly controls the whole seasonal leaf phenology across the pantropical region. Atmospheric dryness is one main type of water stress for leaf phenology during the first half year. However, soil water stress strongly inhibits the first-half of leaf phenology in tropical Asia and the second-half of leaf phenology in Congo, but shows rare constraint on the leaf phenology in Amazon. Ignoring these various roles of soil moisture availability and atmospheric dryness in influencing tropical leaf phenology might lead to unexpected uncertainty for predicting the water and carbon cycles of tropical forest ecosystem in Earth system models.

1. Introduction

Phenology controls on photosynthetic seasonality of the tropical forest biome (Chen et al., 2021; Wu et al., 2016), which accounts for about half of the global forest ecosystem and 34% of global annual terrestrial photosynthesis (Beer et al., 2010). However, tropical trees show a wide range of variations in leaf phenotypic behavior between individuals, species, and locations (Malhado et al., 2009; Yang et al., 2021). These varieties of leaf phenotypic behaviors include entirely leafless for several months, partially losing their leaves for an extended time, dropping and flushing leaves quickly, with continuous leaf turnover throughout the year, and with two periods of leaves dropping and leaf flushing (Croat, 1978; Leigh, 1999; Yang et al., 2021).

Notably, bimodal phenology with two high leaf flush, litterfall, and photosynthesis was observed by both in situ and satellite observations spanning parts of the tropical region (Chen et al., 2020; Wright et al., 1994). For example, Wright et al. (1994) observed bimodal seasonality of leaf flush with peaks in the early dry season and wet season in Barro Colorado Island. The new leaf production of nine tree species in the Bwindi Impenetrable Forest, Uganda followed a bimodal pattern (Shaw, 2016). Two seasonal peaks of leaf flowering were also observed in the tropical moist forest of Uttara Kannada district, Karnataka, India in the years 1983–1985 (Bhat, 1992). The satellite signals, for example, the Enhanced Vegetation Index (EVI), from the Moderate Resolution Imaging Spectroradiometer (MODIS) sensor, also observed a bimodal pattern across evergreen forests in tropical southern America (Xiao et al., 2006) and northwestern Amazon forest (Liang et al., 2015).

Previous debates on the controls of tropical forest phenology mainly vary on the impacts of sunlight and water availability on tropical forest phenology (Guan et al., 2015; Liu et al., 2021). Multiple studies suggest

that water is the main constraint for forest growth during the dry season, and even mild drought can decrease the net carbon uptake with significant leaf abscission and high mortality rates (Asner et al., 2010; Brando et al., 2010; Davidson et al., 2012; Guan et al., 2015; Lewis et al., 2011; Liu et al., 2017, 2021). Ground observations in southern and southwest Amazon show more of a distinct dry season decline in canopy photosynthesis due to water stress (Araujo-Murakami et al., 2014; Malhi et al., 2013; Restrepo-Coupe et al., 2013; Saleska et al., 2009; Vourlitis et al., 2005). But observations from site and satellite signals (Malhi et al., 1998) indicated that some tropical evergreen forests in the northern Amazon increase photosynthesis during the dry seasons with slight water stress due to the deeper rooting system for sufficient groundwater supply (Huete et al., 2006; Morton et al., 2014). Sunlight is regarded as the main limiting factor for tree growth in tropical rainforests (Tang et al., 2017). The enhanced light availability during the early dry season can increase canopy leaf area and total productivity of canopy and emergent trees (Huete et al., 2006; Lee et al., 2013; Tang and Dubayah, 2017; Wright et al., 1994; Wu et al., 2016).

However, the influences of sunlight and water availability on the bimodal phenology across tropical evergreen forests remain poorly addressed (Chen et al., 2020; De Weirdt et al., 2012). In a recent study, Chen et al. (2020) proposed atmospheric dryness as the main water constraint of leaf phenology and photosynthetic seasonality and tested the impact of vapor pressure deficit (VPD) on litterfall and subsequent canopy turnover in the ORCHIDEE model at four Amazon flux tower sites. Results showed good performances for modeling leaf phenology and photosynthetic seasonality at three sites in the central Amazon. But missed the photosynthetic seasonality of the fourth site near the sea in French Guiana with bimodal phenology. Chen et al. (2020) implied that the underlying mechanisms for the two seasonal peaks in tropical phenology might differ greatly and attributed the bimodal phenology to be the main causations for the model failure at the fourth site.

These previous studies justify the necessity in comprehensively assessing the bimodal phenology across tropical forest biome, as well as the underlying causations. The scientific question addressed here was to investigate whether the unimodal and bimodal phenology are mainly controlled by soil water availability, or atmospheric dryness, or sunlight availability in tropical forests. The MODIS EVI and Continuous Solar-induced chlorophyll fluorescence (CSIF) data sets were used to represent the leaf phenology of tropical evergreen forests (Wang et al., 2003; Zhang et al., 2018). The Terrestrial Water Storage (TWS) data from the Gravity Recovery and Climate Experiment (GRACE) was used as the proxy of soil water availability (Humphrey & Gudmundsson, 2019); VPD was used as the proxy of atmospheric water demand as proposed by Chen et al. (2021) and downward short-wave solar radiation (SWdown) was used as the proxy of sunlight availability as proposed by Zhang et al. (2014). On a continental scale, we examined the unimodal and bimodal phenology across tropical evergreen forests using the power spectrum analysis on the time series data of above two phenological proxies, and then we partitioned the seasonality into two periods, the former period from January to June and the later period from July to December (Sections 2.2 and 2.3). To explore separately the seasonal climatic controls of the bimodal phenology, the partial correlation analysis, quadratic fitting analysis and phase analysis were conducted on analyzing the seasonality of phenological proxies against the seasonality of climatic proxies, that is, sunlight, soil water, and atmospheric dryness during the January–June period and July–December period, respectively (Sections 2.4, 2.5 and 2.6). The seasonality of phenological and climatic proxies was all normalized to the Northern Hemisphere.

2. Methods and Materials

2.1. Study Area

Based on the MODIS land cover map (MCD12C1, Sulla-Menashe et al., 2018), we extracted all the pixels that belong to tropical evergreen broadleaf forests (TEF) using the International Geosphere-Biosphere Program (IGBP) classification across pantropical regions at 0.05° spatial resolution from 2007 to 2016. The study area contains three regions: Tropical Asia (15°S–15°N; 92°E–150°E), covering the Indo-China Peninsula and the majority of the Malay Archipelago, Congo (15°S–15°N; 10°E–30°E), the western part of the Africa TEF region, and Amazon (15°S–15°N; 50°W–80°W), the world's largest and most biodiverse tropical rain forest.

Table 1
Data Sources for Phenological and Climatic Proxies

	Proxy	Parameter	Full name	Data source/version	Spatial/ temperol resolution	Period	Reference
Phenology	photosynthesis	EVI	enhanced vegetation index	MODIS(MYD13C2)	0.05°/monthly	2007–2016	Didan, 2015
		CSIF	global spatially contiguous SIF	Continuous Solar-induced chlorophyll fluorescence	0.05°/4-days	2007–2016	Zhang et al., 2018
Climate	Soil water availability	TWS	Terrestrial Water Storage	GRACE_REC_v03	0.5°/monthly	2007–2016	Humphrey and Gudmundsson, 2019
	Sunlight availability	SWdown	short-wave incoming radiation	CRUNCEP	0.5°/monthly	2007–2016	Viovy, 2018
	Atmospheric water demands	VPD	vapor pressure deficit	ERA-Interim	0.5°/monthly	2007–2016	Yuan et al., 2019

2.2. Data Sets

The gridded photosynthesis and climate products from remote sensing and modeling in this study were summarized in Table 1. All data sets were aggregated at the same spatial (0.5°) and temporal (monthly) resolutions.

2.3. Power Spectrum Analysis

Plancherel's theorem states that the total energy of a signal remains the same after the Fourier transform (Wiener, 1988). The power spectrum is obtained by dividing the square of the amplitude modulus by the number of sampling points. Power spectrum analysis uses the fast Fourier transform to expand time signals in spectral space and decomposes the total energy of time series into the energy of different frequencies.

In this paper, the power spectrum analysis based on fast Fourier transform operation was applied to convert the amplitude spectrum to power spectrum (Juárez & Liu, 2001) and then to detect the frequency of phenological proxy cycles, in each pixel on the time series data of phenological proxies (EVI and CSIF) from 2007 to 2016. The frequency index is represented by an integral number i, whose value varies from 1 to 6. If the frequency i equals to 1, the phenological proxy occurred *once* times a year and the type was defined as *annual cycle*; and if the frequency i equals to 2, the phenological proxy occurred *twice* a year and the type was defined as *half-year cycle*. If the ratio (R_i) of the power for the given frequency i to the total power of time series is greater than or equals to 50%, the phenological proxy mainly cycles i times a year. The sum of $R_i\left(\sum_{i=0}^{6} R_i\right)$ equals to 1.0.

Here, we defined the phenological types using the criteria:

1. When $R_2 > 50\%$, the pixel shows a bimodal half-year cycle phenology;
2. When $R_1 > 90\%$, the pixel shows a unimodal annual cycle phenology;
3. When $50\% < R_1 < 90\%$, the pixel shows a bimodal annual cycle phenology. The larger the R_1 value is, the greater probability the phenology is close to the unimodal annual cycle phenology; the smaller the R_1 value is, the greater probability the phenology is close to the half-year cycle phenology.

2.4. Phase Analysis of Water Stress Factors Against Photosynthetic Indicators

Before the phase analysis, we calculated the canopy fluorescence yield (F_{CSIF}) — an index shown to respond to seasonal variations of photosynthesis (Zeng at al., 2019) from CSIF divided by the absorbed photosynthetically active radiation (APAR), as Equation 1. Based on MODIS EVI, we also calculated a similar index—F_{EVI} using Equation 2.

$$F_{CSIF} = \frac{CSIF}{APAR} \quad (1)$$

$$F_{EVI} = \frac{EVI}{APAR} \quad (2)$$

where the APAR is calculated from product of photosynthetically active radiation (PAR) (MJ m^{-2}) and fraction of PAR absorbed by the vegetation (fPAR) influenced by the phenological cycle.

After that, the cross-correlation function method (Luo et al., 2003) was used to calculate the phase difference between the seasonal series of photosynthetic indexes (F_{EVI} and F_{CSIF}) and water stress factors (VPD and TWS), to check which type of water stresses controls the leaf phenology. The time series data of the photosynthetic indexes are set as $A(\ )$ and the time series of the climate factor are set as $B(\ )$. Then, the function of cross-correlation (r_{AB}) is calculated as Equation 3.

$$r_{AB} = \sum_0^N A(i)B(i+m) \quad (3)$$

where N is the total number of samples. is from 0 to N. $m = -N, -N+1, \cdots\cdots N-1, N$.

When r_{AB} reaches the maximum, the corresponding m value is the delay of $B(n)$ relative to $A(n)$. That's the phase difference between $B(n)$ and $A(n)$. When $m > 0$, it means that $B(n)$ is ahead of $A(n)$, otherwise it means that $B(n)$ is behind $A(n)$.

Bradley et al. (2011) showed that if the seasonal cycle of a given climate factor is earlier than or in the same period with the seasonal cycle of phenology, the given climatic factor may drive seasonal phenological changes. Similarly, if the phase of a water stress factor shortly precedes that of F_{EVI} and F_{CSIF}, for example, the corresponding water stress proxy will be treated as a potential water constraint driving the phenology seasonal cycle of F_{EVI} and F_{CSIF}.

It should be noted again that, for the bimodal phenology, we divided the seasonality into two periods (January–June and July–December); and analyzed separately the phase differences between phenological proxies and water stress factors for each period, to reveal which types of water stresses, that is, atmospheric dryness or soil water deficit, dominates the water constraints for each part of the bimodal phenology.

2.5. Quadratic Fitting Analysis

After dividing the seasonality of phenological proxies into two periods, a quadratic fitting of phenological proxies or climate factors with month was conducted on each pixel for each period, that is, January–June or July–December, respectively. The formula of the quadratic fitting was expressed as:

$$PP = A \times (t - t_{max})^2 + pp_{max} \quad (4)$$

where PP represents the seasonal values of phenological proxies; represents the time in unit of the month, that is, from 1 to 12; A is a coefficient, representing the opening direction and size of the quadratic curve; pp_{max} represents the peak value of seasonal phenological proxies; t_{max} represents the month corresponding to pp_{max}.

Figure 1 is an illustration graph for the quadratic fitting analysis of photosynthetic (EVI and CSIF) and climatic proxies (VPD, SWdown, and TWS) for the January–June period and July–December period. The orange, blue and rose curves represent three types of seasonality of photosynthetic or climatic proxies. The differences in the two maximum values (pp_{max}) of seasonal photosynthesis between two curves indicate that the seasonal maximum photosynthesis differ between pixels with different R_i, which are caused by different pp_{max} of climatic drivers. So, we divided the seasonality into two periods (January–June and July–December) and then used quadratic fitting analysis to fit the curve of phenological proxies and climatic factors for the January–June period and July–December period, respectively. After that, we conducted the partial correlation analyses between the pp_{max} of a given photosynthetic proxy and that of a given climatic proxy, using all the pixels across the pantropical TEF, to investigate separately the impacts of atmospheric water vapor pressure deficit, soil water availability, and sunlight availability on tropical forests photosynthesis.

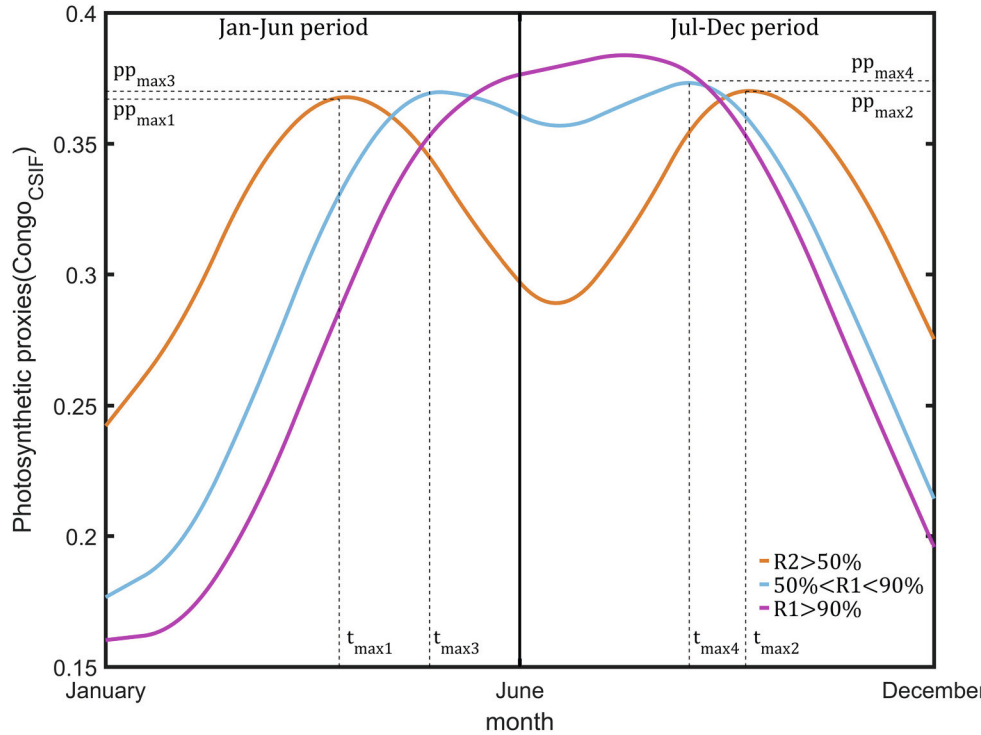

Figure 1. Illustration for the quadratic fitting analysis of photosynthetic or climatic proxies for the January–June period and July–December period, respectively. The pp_{max} represents the peak value and t_{max} represents the time to reach the peak value. For examples, for photosynthetic proxies, the orange curve represents the bimodal 6-month cycle phenology with $R_2 > 50\%$. The blue curve represents the bimodal annual cycle phenology with $50\% < R_1 < 90\%$. The rose curve represents the unimodal annual cycle phenology with $R_1 > 90\%$.

2.6. Partial Correlation Analysis

Partial correlation analysis refers to that in a system composed of multiple elements, when the influence or correlation degree of one element on another is studied, the influence of other elements is temporarily ignored and the degree of mutual relationship between the two elements is solely studied (Zheng & Liu, 1986). Assuming that we need to calculate the correlation between X and Y, where Z represents all the other variables, the partial correlation coefficient between X and Y can be thought of as a simple correlation coefficient between the residuals R_X from the linear regression of X and Z and the residuals R_Y from the linear regression of Y and Z. The residual R_X is added to the mean value of X to obtain P_X, which eliminates the influence of Z variable. Here, we use the partial regression analysis to partition the coupling impacts of climate factors on leaf phenology.

3. Results

3.1. Latitudinal Patterns of Unimodal and Bimodal Phenology Across Pantropical Evergreen Forests

See in Figure 2, we evaluated the differences in the phenological changes of CSIF and MODIS EVI for each pixel and calculated the correlation coefficients (Cor) between CSIF and MODIS EVI on time-series data. Results show that 99.68% of the pixels show positive correlations between seasonal CSIF and EVI and values of the correlation coefficient is even bigger than 0.4 in 97.82% of the pixels, which imply consistent phenological changes between CSIF and MODIS EVI across the whole TEF region. Particularly, 68.67% (Figures 3a–3f) of the TEF pixels across the pantropical region show the annual cycle phenology and 31.30% (Figures 3a–3f) show the 6-month cycle phenology; while only 0.03% (Figures 3a–3f) of the TEF pixels show other types of cycles in canopy phenology.

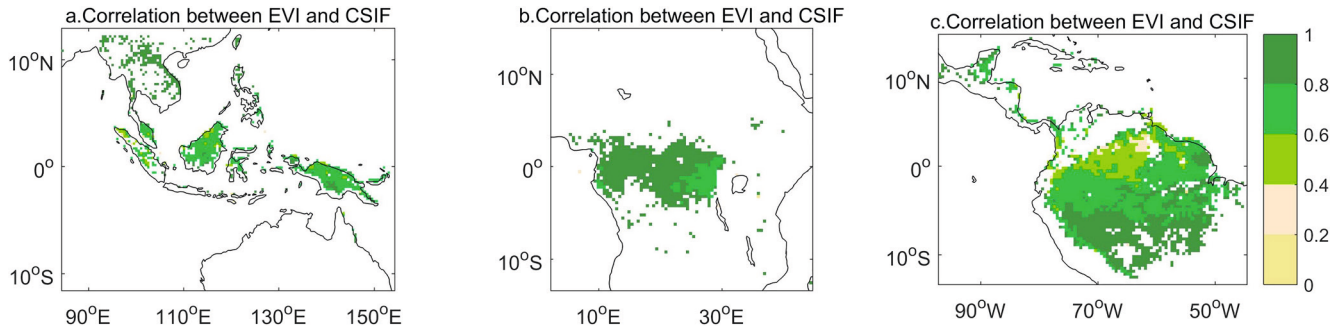

Figure 2. Correlation of photosynthetic proxies (Enhanced Vegetation Index [EVI] and Continuous Solar-induced chlorophyll fluorescence [CSIF]) in tropical forests.

Figure 4 shows the periodic biological phenomena of two photosynthetic proxies, that is, EVI, CSIF across Amazon, Congo, and Asia, respectively. The pixels in a 6-month cycle with $R_2 > 50\%$ present significant bimodal phenology (orange curve). The two peaks occurred around March and September, respectively, and the valley occurred around June. However, the pixels in an annual cycle with $R_1 > 90\%$ present significant unimodal phenology (rose curve) and the peak occurred around August. The pixels in an annual cycle with R_1 equaling to 50%–60%, 60%–70%, 70%–80%, 80%–90%, >90% vary gradually from bimodal annual phenology to unimodal annual phenology, implying that the larger the R_1 value is, the greater probability the phenology is close to annual cycle seasonality.

Figure 5 shows the spatial patterns of bimodal and unimodal phenology of the two photosynthetic proxies across Asia, Congo, and Amazon, respectively. The results show that tropical forests near the equator (3°S–3°N) mostly have a 6-month bimodal cycle (orange), and are mainly distributed in Indonesia in Asia, south-central Congo, and northern Amazon. The probability (R_1) of the phenological cycle as an annual cycle type increases from the equator to the northern and southern higher latitudes (3°N–15°N, 3°S–15°S).

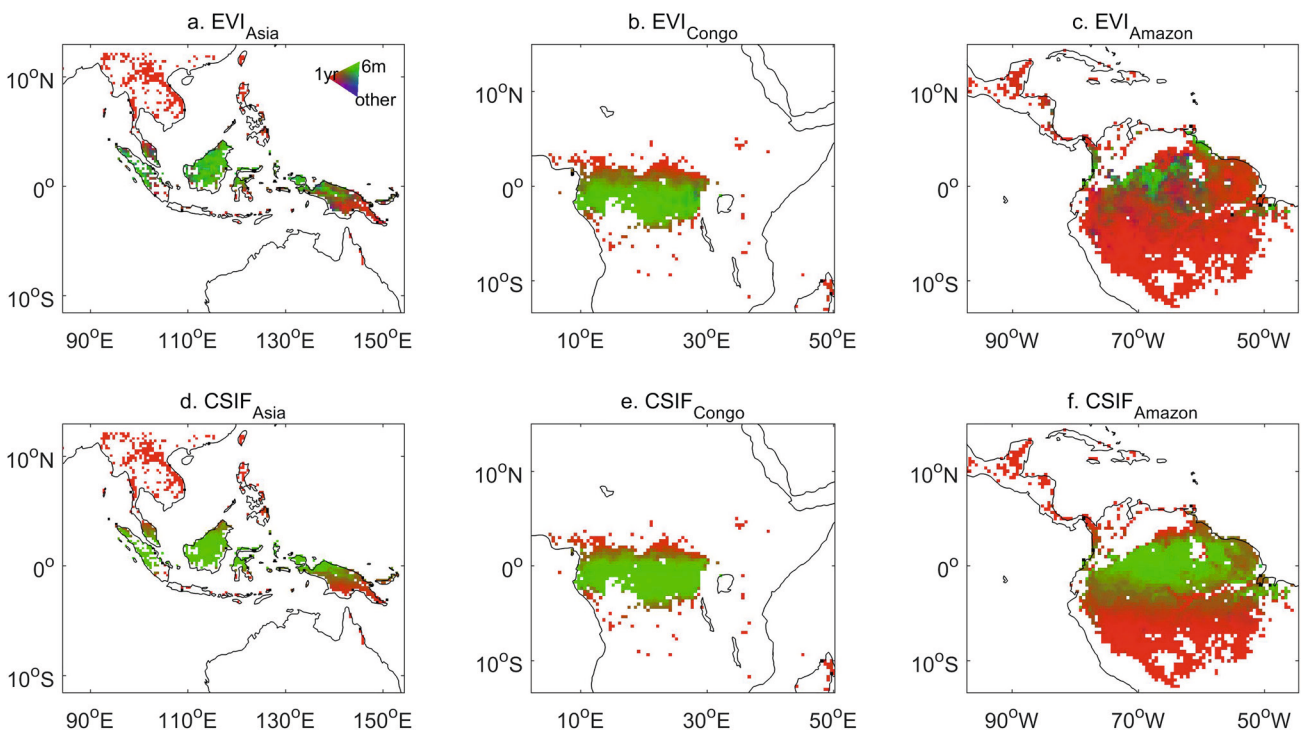

Figure 3. Seasonal variations of Enhanced Vegetation Index (EVI) and Continuous Solar-induced chlorophyll fluorescence (CSIF) in 6-month cycle (R_2 value > 50%) and annual cycle (R_1 > 50%).

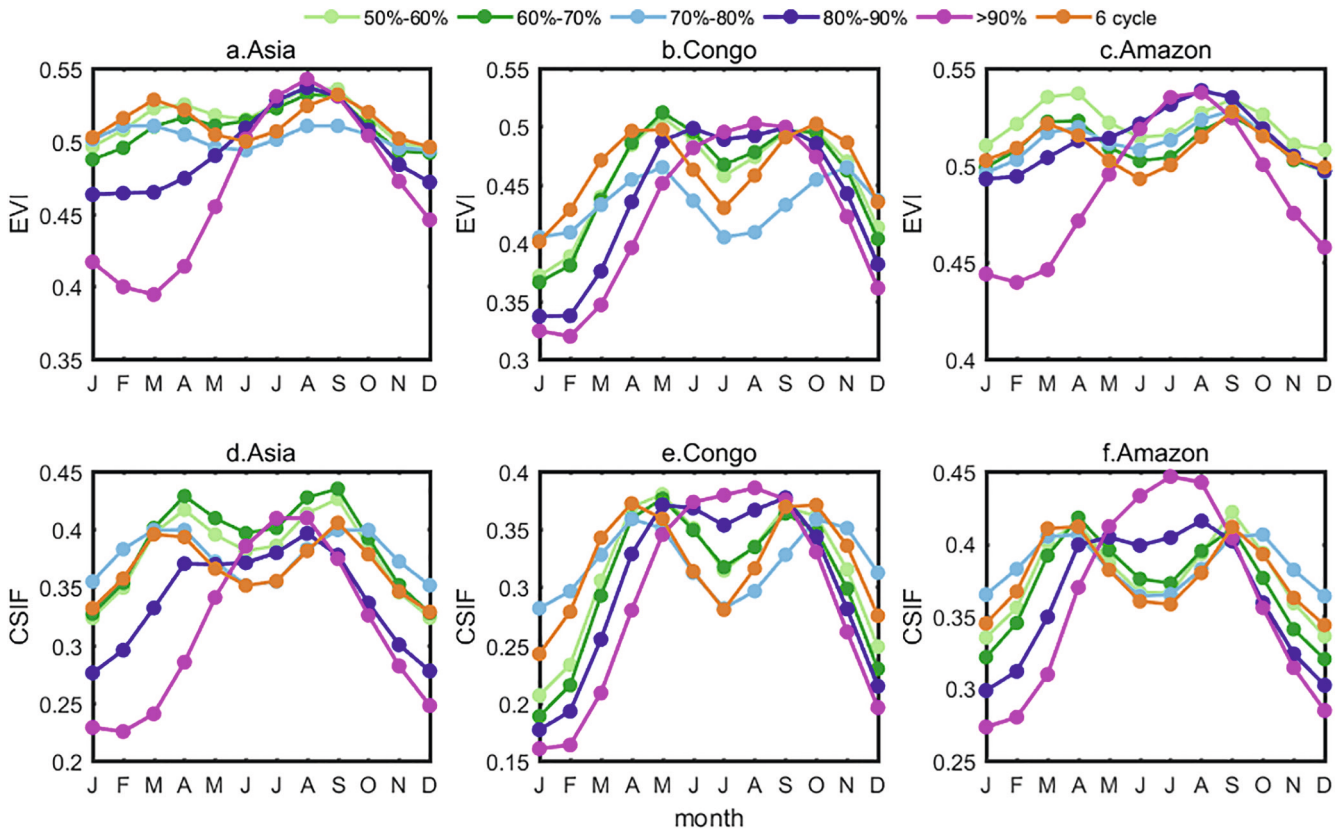

Figure 4. Seasonal variations of Enhanced Vegetation Index (EVI) and Continuous Solar-induced chlorophyll fluorescence (CSIF) in bimodal phenology and unimodal phenology. The 6-month cycle with $R_2 > 50\%$ and annual cycle with $50\% < R_1 < 90\%$ are more like bimodal phenology; and annual cycle with $R_1 > 90\%$ (rose color) are more like a unimodal phenology.

The pixels with unimodal phenology are mainly located in higher latitudes (>5°N, >5°S). Notably, the two photosynthetic proxies, that is, EVI and CSIF, show similar patterns across the tropical region.

3.2. The Unimodal and Bimodal Seasonality of Climatic Factors

We further draw the seasonality of climatic proxies (VPD, SWdown, and TWS) for each sub-region in a 6-month cycle and annual cycle with different R_1 respectively. Results are shown in Figure 6. In general, the periodic phenomena of three climatic proxies show similar seasonal patterns as those of photosynthetic proxies, respectively.

The pixels with bimodal phenology present a significant bimodal seasonality of SWdown (orange curve) with two peaks occurring in March and September and valleys occurring in June; while the pixels with unimodal phenology correspondingly present a unimodal seasonality of SWdown (rose curve) with a peak occurring in April (Figures 6b, 6e, and 6h). As the values of R_1 increases from 50%–60%, 60%–70%, 70%–80%, 80%–90%, to >90%, the SWdown seasonality changes gradually from a bimodal seasonality to a unimodal seasonality. Importantly, the first peak of SWdown increases as R_1 increases during the January–June period; while the second peak of SWdown decreases as R_1 increases during the July–December period. The VPD and TWS both show a unimodal seasonality. The peak of VPD happens around February and its value increases with R_1 increases (Figures 6a, 6d, and 6g). On the contrary, the peak of TWS happens around October during the July-December period and its value increases also with R_1 increases (Figures 6c, 6f, and 6i).

To quantitively assess the seasonal differences between the seasonality curve of climatic and photosynthetic proxies, we conducted a quadratic fitting analysis between phenological proxies (EVI and CSIF) and climate factors (VPD, SWdown, and TWS) based on each pixel in the tropics for the January–June period and July–December period (Section 2.5). We analyzed the relationship between the seasonal peak value (pp_{max})

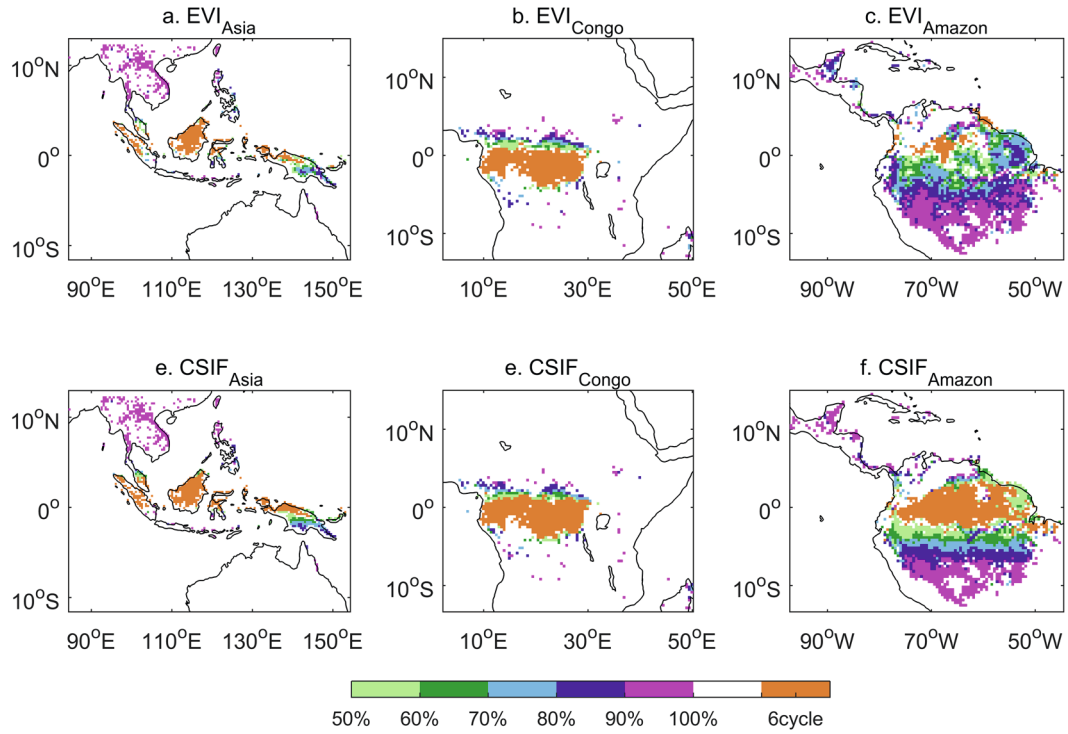

Figure 5. Seasonal variations of Enhanced Vegetation Index (EVI) and Continuous Solar-induced chlorophyll fluorescence (CSIF) in bimodal phenology and unimodal phenology. The 6-month cycle with $R_2 > 50\%$ and annual cycle with $50\% < R_1 < 90\%$ are more like bimodal phenology; and annual cycle with $R_1 > 90\%$ (rose color) are more like a unimodal phenology.

of phenological proxy and climate factors to investigate separately the impacts of VPD, SWdown, and TWS on tropical forests photosynthesis.

3.3. Climatic Controls of Leaf Phenology Across Pantropical Evergreen Forests

3.3.1. Sunlight Controls the Seasonal Leaf Phenology in Certain Areas of Tropical Asia and Atmospheric and Soil Water Stresses Show Strong Constraints on the First Half of Phenological Seasonality

In tropical Asia, during the January–June period, the pp_{max} of VPD is negatively correlated to those of phenology proxies (EVI and CSIF) for all sub-regions (Figure 7). TWS is in contrast positively correlated to those of phenology proxies, especially in high-latitude sub-regions with $70\% < R_1 < 90\%$ (Figure 7e). During the July–December period, the pp_{max} of VPD and TWS both show no significant correlation with those of phenology proxies (Figures 7b and 7f). Analyses indicate that the pp_{max} of SWdown is positively correlated to that of phenological proxies in some sub-regions during both the January–June period and July–December period, but these sub-regions varied greatly between different phenology proxies (Figures 7c and 7d).

Above analyses indicate that atmospheric dryness and soil water deficit jointly control the water constraints of first half leaf phenology in tropical Asia. To further examine this water constraint hypothesis for each part of the bimodal phenology, the phase analysis is conducted on water stress proxies (VPD and TWS) to analyze against those of F_{EVI} and F_{CSIF} during the January-June period and July-December period, separately (Method: Section 2.4). If the seasonality of a given water stress factor in phase or leads to that of the phenological proxy, this factor will be considered as a potential controlling water constraint to inhibit the seasonal cycle of tropical forest phenology. In general, the seasonality of VPD and TWS are in phase with or leads to those of F_{EVI} and F_{CSIF} except for pixels in the sub-region with a 6-month cycle during the January–June period (Figure 8). However, the phase of VPD and TWS in most sub-regions lag behind that of F_{EVI} and

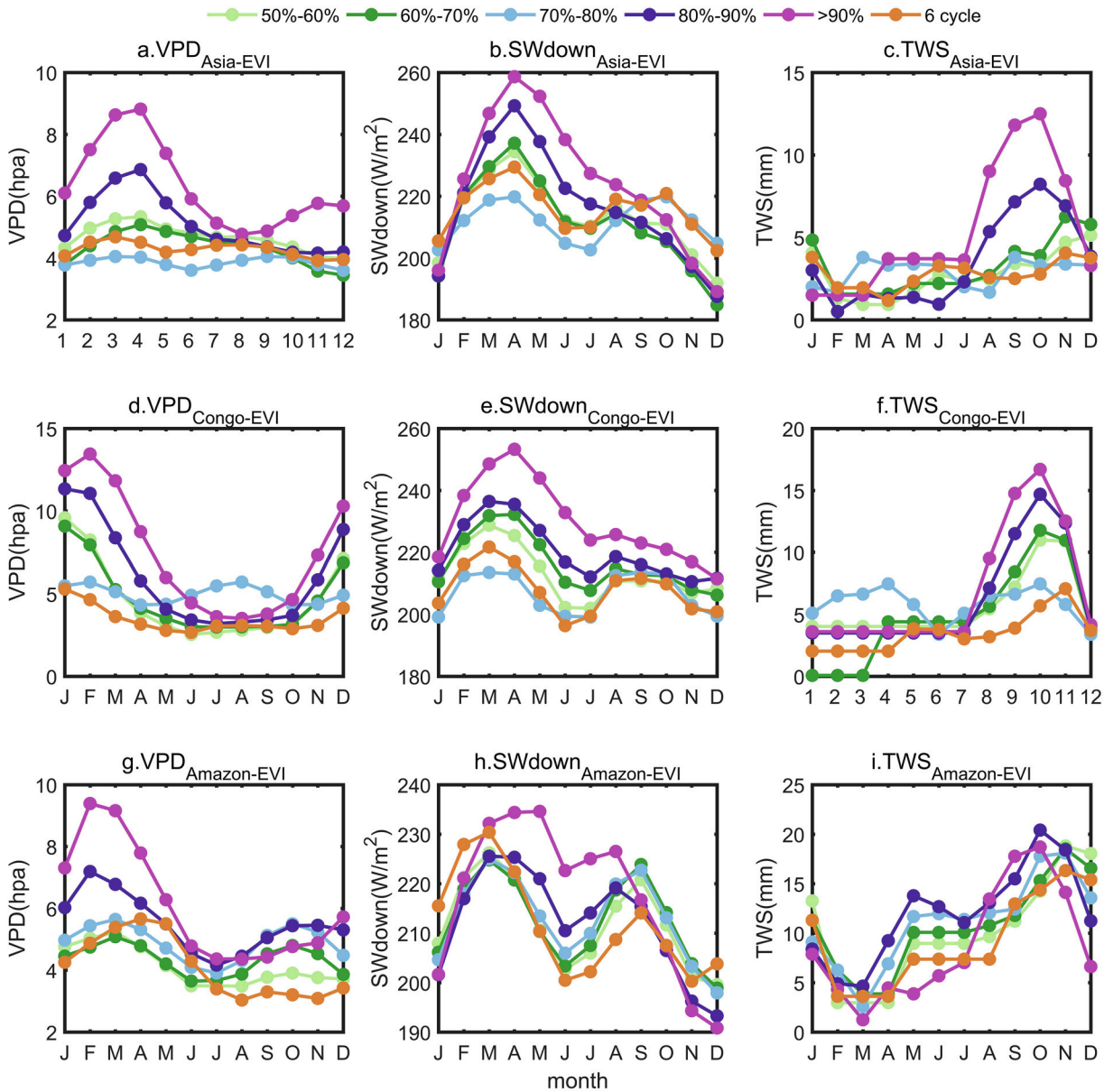

Figure 6. Seasonal variation of climatic proxies (vapor pressure deficit [VPD], downward short-wave solar radiation [SWdown], and Terrestrial Water Storage [TWS]) for sub-regions in 6-month cycle and annual cycle with different R_1.

F_{CSIF} during the July–December period. The phase analyses support that atmospheric and soil water stress jointly constrain on the first half of photosynthesis seasonality across pantropical Asia.

3.3.2. Sunlight Dominantly Controls the Whole Seasonal Leaf Phenology and Atmospheric Dryness Constrains on the First Half and Soil Water Stress Constrains on the Second Half of Phenological Seasonality in Congo

In the Congo region, the pp_{max} of SWdown is strongly positively correlated to those of EVI and CSIF during the whole period (Figures 9c and 9d). The pp_{max} of EVI and CSIF show a negative relationship with VPD during January-June period (Figure 9a); but shows mostly no significant correlations with VPD during the July-December period (Figure 9b). Atmospheric water stress is the main type of water limitations on the first half of leaf phenology of tropical evergreen forests in Congo. On the contrary, the values of the first peak in EVI and CSIF show no significant variations as the pp_{max} of TWS changes, implying weak correlation between TWS and phenological proxies during the January–June period (Figure 9e). During the

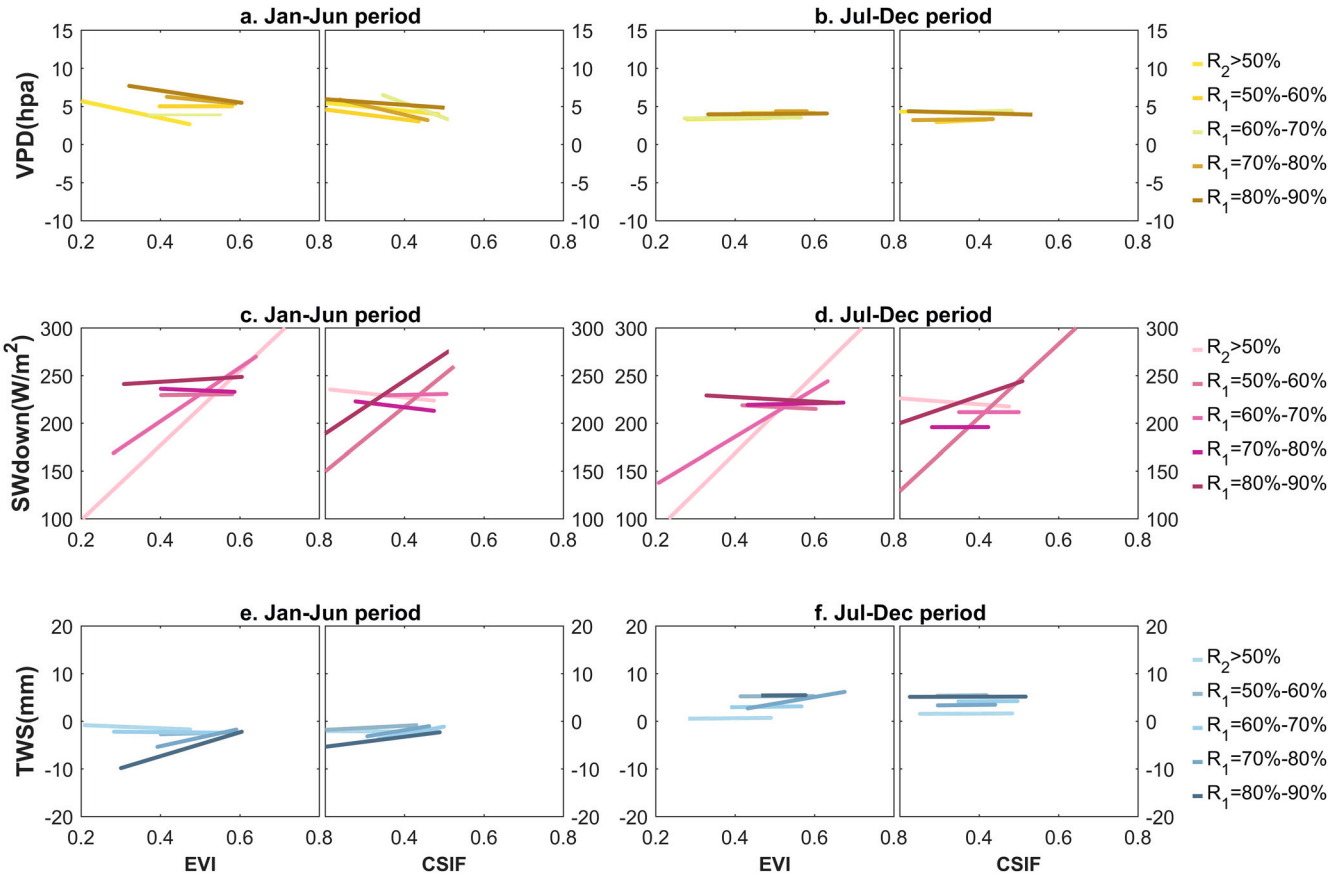

Figure 7. The linear fitting curves between peak values (pp_{max}) of phenological proxies (Enhanced Vegetation Index [EVI] and Continuous Solar-induced chlorophyll fluorescence [CSIF]) and that of climatic factors in the Asia region based partial correlation analyses during the January-June period and July-December period, respectively. The corresponding scatter diagrams between peak values (pp_{max}) of phenological proxies (EVI and CSIF) and that of climatic factors were shown in Figures S1–S4.

July–December period, the soil water availability is strongly positively correlated to those of EVI and CSIF, especially in high latitudes (Figure 9f).

Additionally, phase analysis shows that (Figure 10), during the January-June period, the seasonality of VPD mostly leads or is in phase with that of F_{EVI} and F_{CSIF}; while the seasonality of TWS always lags behind that that of EVI and CSIF (Figures 10a, 10c, 10e, 10g, and 10i). The water stress conditions convert during the second half of year. The phase of soil water factors (etc., TWS) precedes that of F_{EVI} and F_{CSIF} during the July-December period. However, the seasonality of VPD is always latter in phase than that of F_{EVI} and F_{CSIF} (Figures 10b, 10d, 10f, 10h, and 10j). Therefore, according to the quadratic fitting and phase analyses, sunlight availability and atmospheric dryness jointly regulate the seasonal variations of plant photosynthesis from January to June period; while sunlight and soil water availability jointly influence the seasonal photosynthesis from July to December across Congo tropical forests.

3.3.3. Sunlight Controls the High-Latitude Leaf Phenology and Atmospheric Dryness Exhibits Strong Water Constraints on the First Half of Phenological Seasonality in Amazon

In Amazon, the situation is much complex. The quadratic fitting analysis shows that the pp_{max} of SWdown is strongly positively correlated to those of EVI and CSIF, especially in high latitudes (Figures 11c and 11d). During the January-June period, the pp_{max} of VPD is negatively correlated to those of phenology proxies (EVI and CSIF) (Figures 11a), similar as that of Congo. However, during the July–December period, the pp_{max} of VPD and TWS both show no significant correlations with those of phenology proxies (EVI and CSIF) (Figures 11b and 11f), similar as that of tropical Asia.

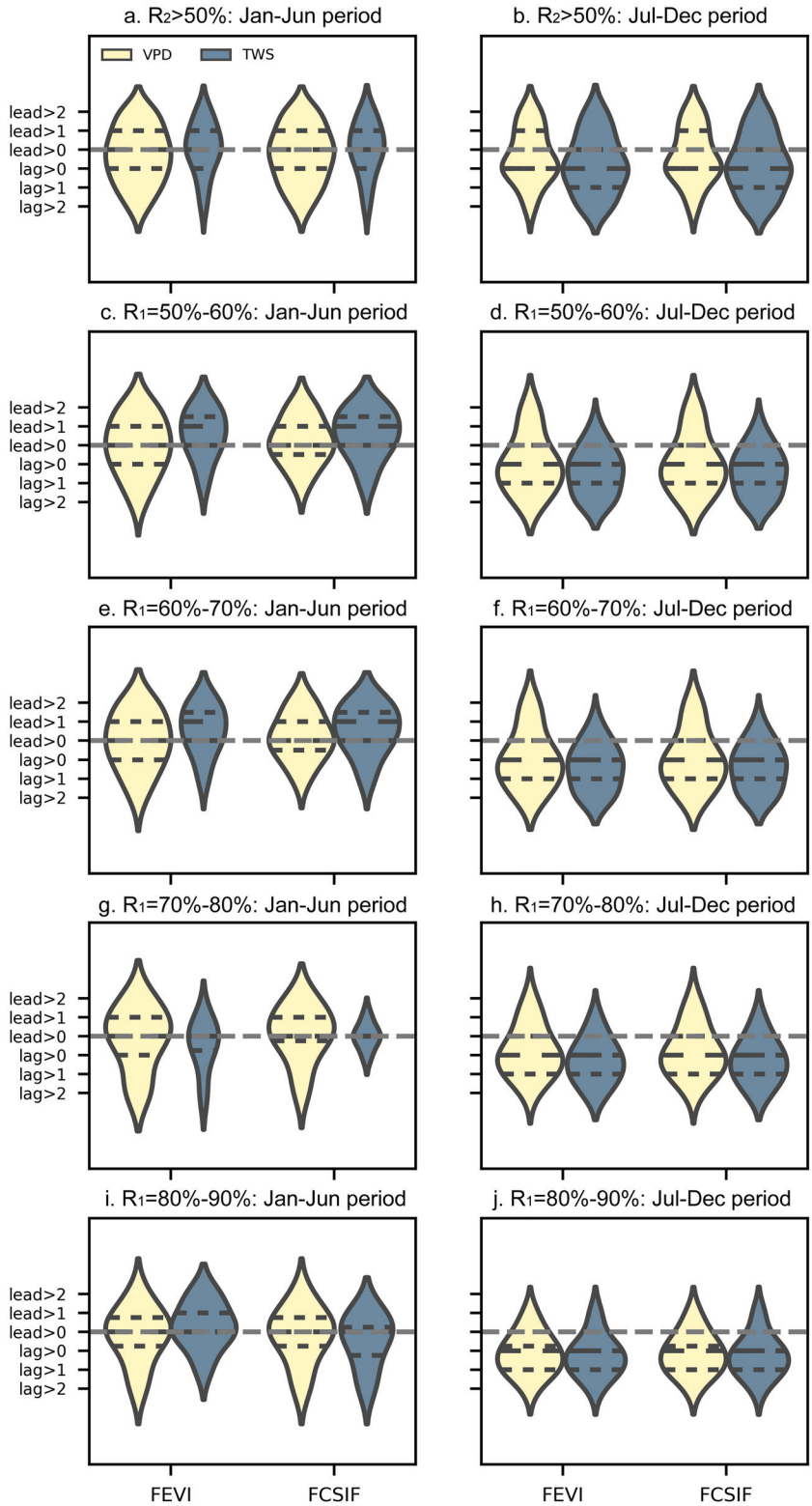

Figure 8. Phase difference between F_{EVI}, F_{CSIF} and water stress factors (vapor pressure deficit [VPD] and Terrestrial Water Storage [TWS]) in tropical Asia during the January–June period and July–December period, respectively.

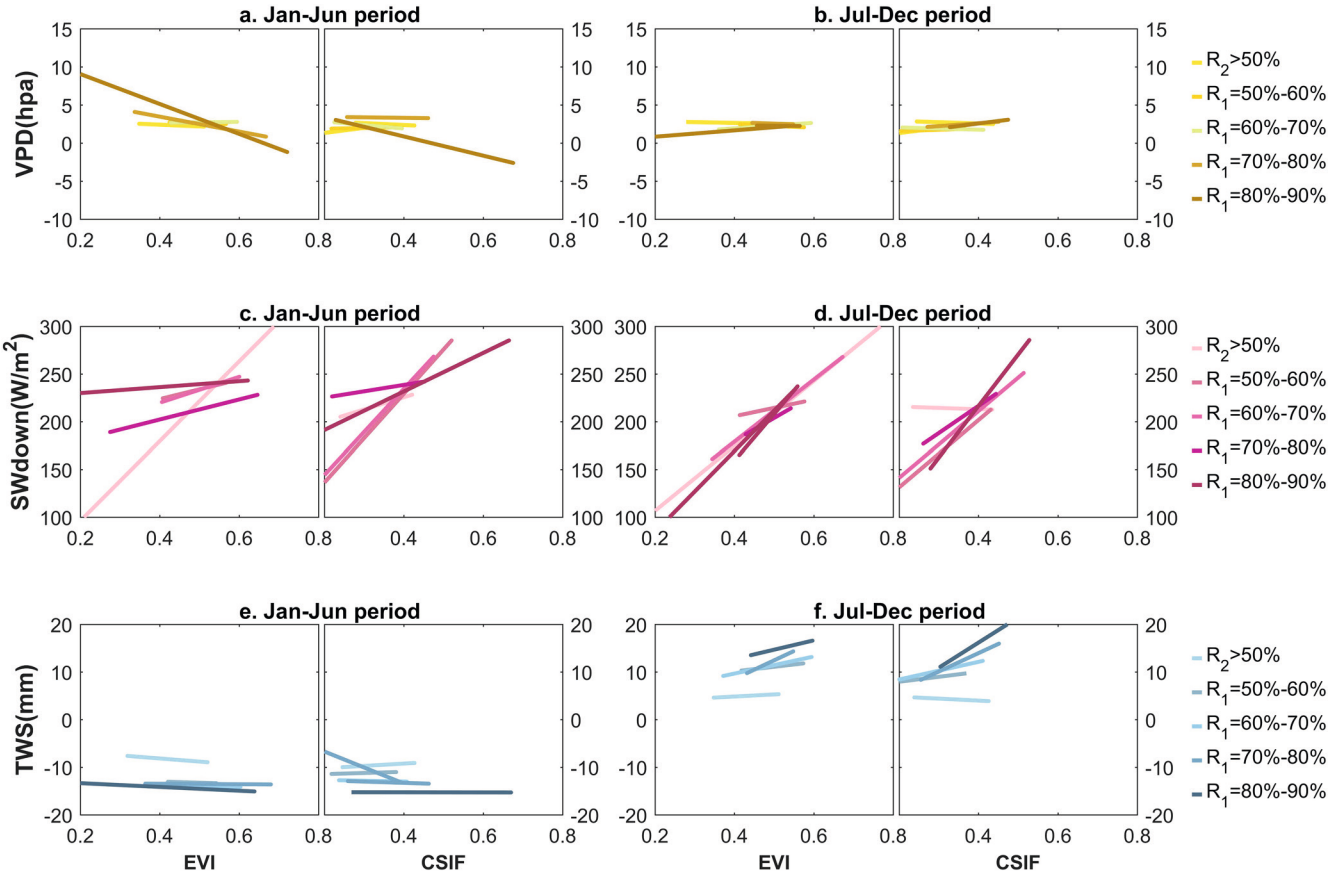

Figure 9. The linear fitting curves between values (pp_{max}) of phenological proxy (Enhanced Vegetation Index [EVI] and Continuous Solar-induced chlorophyll fluorescence [CSIF]) and that of climatic factors in the Congo region based partial correlation analyses during the January-June period and July-December period, respectively. The corresponding scatter diagrams between peak values (pp_{max}) of phenological proxies (EVI and CSIF) and that of climatic factors were shown in Figures S5–S8.

The phase-analysis shows that, VPD mostly leads or is in phase with that of F_{EVI} and F_{CSIF} during the January-June period and TWS mostly lags behind that of F_{EVI} and F_{CSIF} (Figures 12c, 12e, 12g and 12i). However, both VPD and TWS are latter in phase than F_{EVI} and F_{CSIF} during the July–December period (Figures 12b, 12d, 12f, 12h, and 12j). In summary, for Amazon tropical forests, sunlight availability generally shows dominantly impacts on the leaf phenology; and atmospheric water availability plays more important role in the first half of year; however, both soil and atmospheric water stress show rare impacts on the second half of phenological seasonality.

4. Discussion

Current studies widely debate on the seasonal controls of sunlight and water availability on the seasonal changes of tropical forest phenology. This can be well explained by a cost-benefit theory (Kikuzawa, 1991), where adaptive strategies of shedding and producing leaves are seen as a response to light and water availability. With less constraints from soil moisture deficit and atmospheric water deficit, trees will flush new efficient leaves in the sunnier season to maximize light capture and productivity (Brando et al., 2010; Davidson et al., 2012; Wu et al., 2016; Lopes et al., 2016). When plants suffer constraints from either soil moisture deficit or atmospheric water deficit, trees accelerate leaf abscission to minimize the costs and avoids hydraulic failure (Brodribb et al., 2002; Lee & Boyce, 2010).

It is worth noting that water stresses can cause drought (Liu et al., 2017, 2021) and produce abscisic acid, which promotes leaf shedding (Oguntunde, 2005), but increasing sunlight is not likely to produce abscisic acid. For examples, previous studies found that the leaves shed after experiencing a drop in the

10.1029/2021EF002160

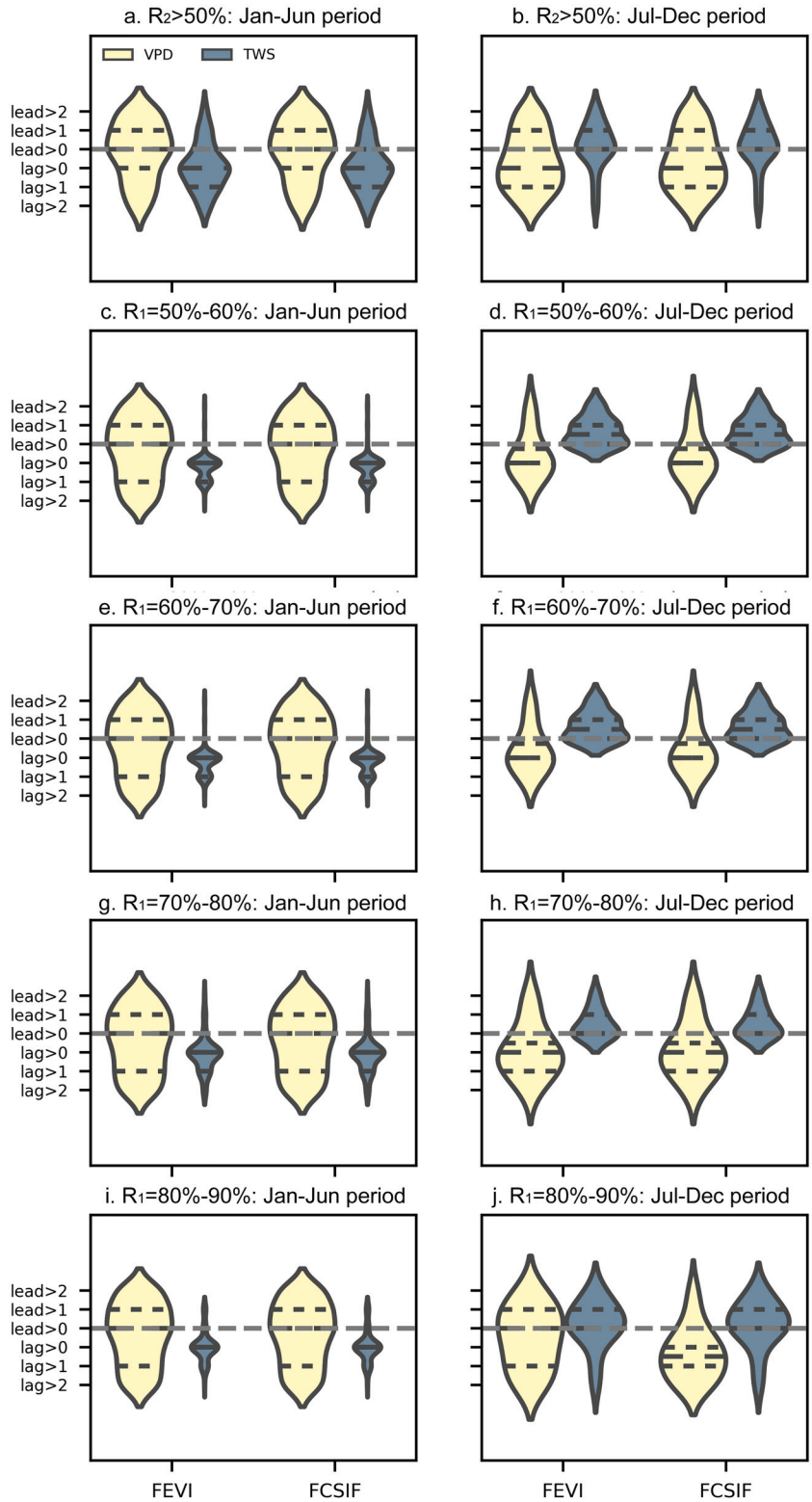

Figure 10. Phase difference between F_{EVI}, F_{CSIF} and water stress factors (vapor pressure deficit [VPD] and Terrestrial Water Storage [TWS]) in Congo during the January–June period and July–December period, respectively.

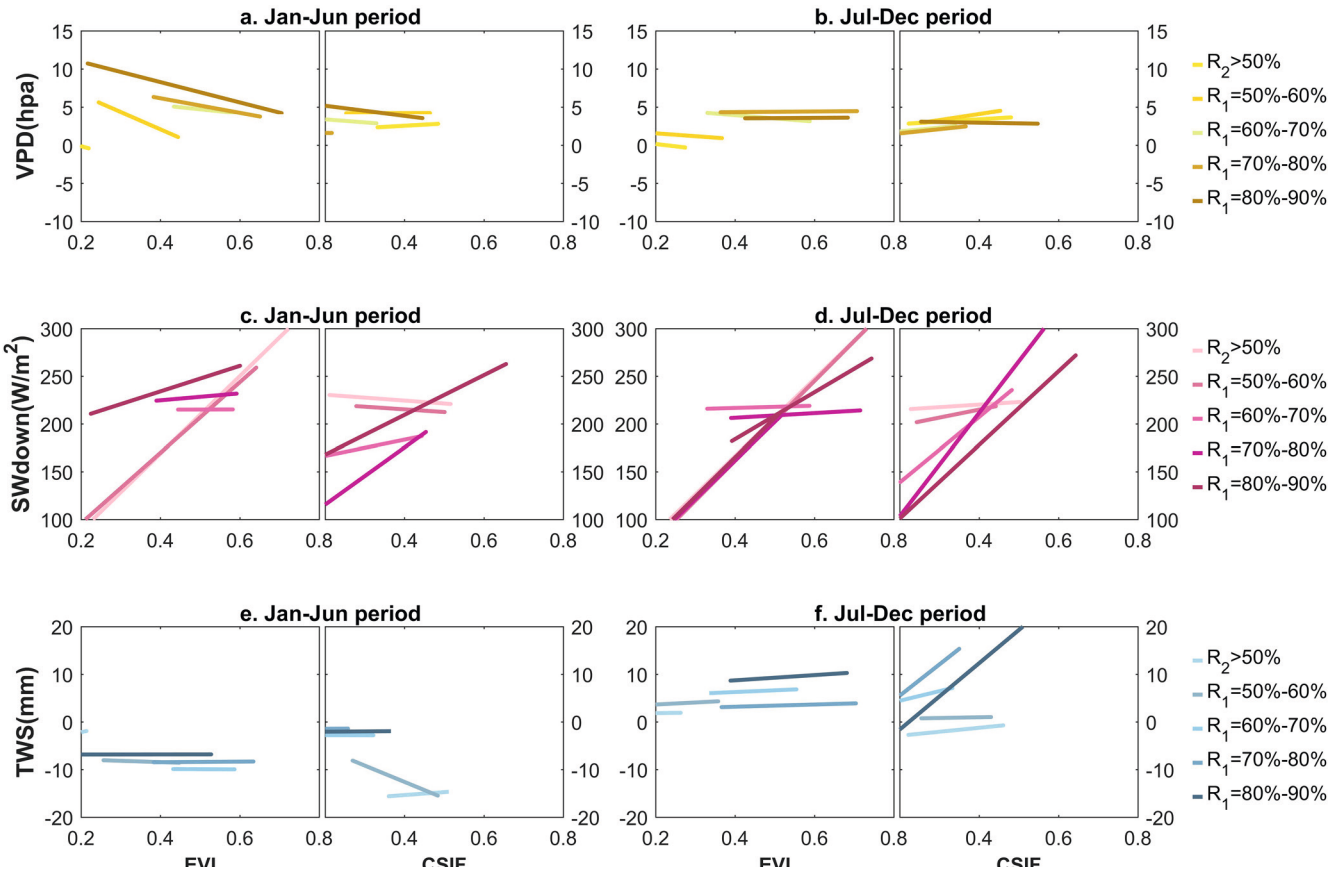

Figure 11. The linear fitting curves between values (pp_{max}) of the phenological proxy (Enhanced Vegetation Index [EVI] and Continuous Solar-induced chlorophyll fluorescence [CSIF]) and that of climatic factors based partial correlation analyses in the Amazon region during the January-June period and July-December period, respectively. The corresponding scatter diagrams between peak values (pp_{max}) of phenological proxies (EVI and CSIF) and that of climatic factors were shown in Figures S9–S12.

photosynthetic rate at the end of the rainy season (Taiz & Zeiger, 2002; Zhang et al., 2014). However, the effect of SWdown on litterfall has not been partitioned from soil and atmospheric water availability when empirically analyzing the relationship between sunlight and litterfall seasonality. In larger parts of tropical regions, sunlight and VPD and soil moisture always show consistent seasonal phases (Chen et al., 2020). It might result in a fake causal link between sunlight and litterfall seasonality. This study based on partial correlation analysis rather supports that the accompanied low soil water content or high atmospheric dryness might be the main causations for leaf shedding; while sunlight likely controls on the leaf flushing processes. For examples, observations have also shown that with the onset of the dry season, sunlight begins to increase again, which usually coincides with the production of new leaves (Descheemaeker et al., 2006; Moraes et al., 1999).

The roles of soil moisture availability and atmospheric dryness in controlling the plant water constraints have not been well documented across the pantropical region. Multiple studies suggested that soil water deficit is the main constraint for forest growth during the dry season (Brando et al., 2010; Guan et al., 2015; Lewis et al., 2011). However, Chen et al. (2020, 2021) tested the seasonality of precipitation, SWdown, and VPD as climate triggers of litterfall and suggested that VPD was the best empirical trigger for old leaf shedding across Amazonian evergreen broadleaved forests. Actually, high VPD or low soil moisture can both cause plants to close their stomata to prevent water loss, thus inhibiting photosynthesis (Zhou et al., 2019). Chen et al.'s (2020) phenology module failed at the fourth site off the shore of the Guiana coast, and suggested that it might be related to bimodal phenology in the forests off the coast of Guiana. In this study, results strongly confirm the above-mentioned bimodal phenology hypothesis. The key finding here is that the two peaks of tropical leaf phenology tend to be dominated by different types of water stresses. In tropical

10.1029/2021EF002160

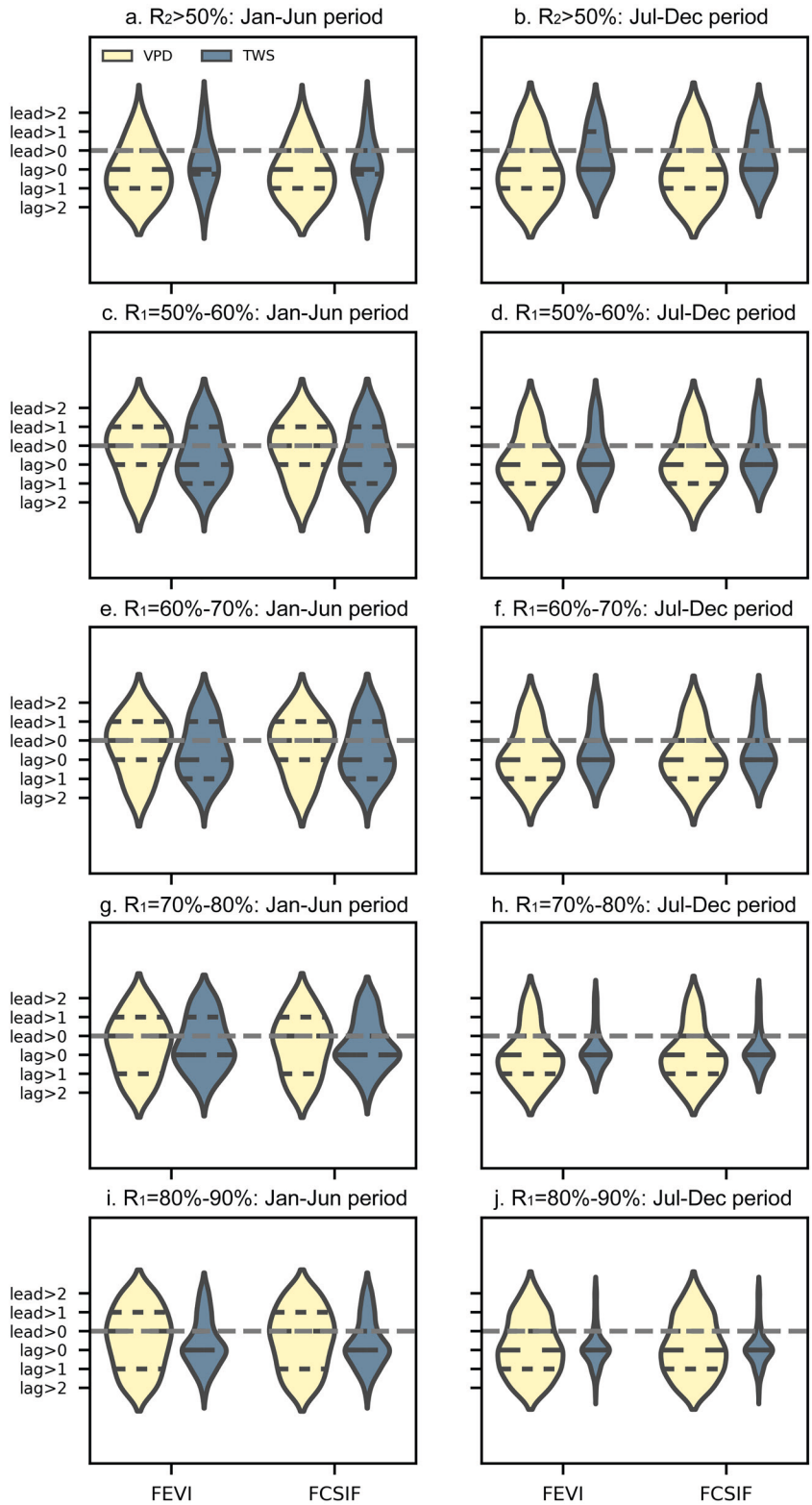

Figure 12. Phase difference between F_{EVI}, F_{CSIF} and water stress factors (vapor pressure deficit [VPD] and Terrestrial Water Storage [TWS]) in Amazon during the January–June period and July–December period, respectively.

Asia, atmospheric and soil water stress jointly constrain on the first half of leaf phenology; while in Congo atmospheric dryness and soil water stress act as dominant water constrains on the first and second half of phenological seasonality, respectively. However, atmospheric dryness is the main type of water stress during the first half of leaf phenology in Amazon. Therefore, ignoring these different influences of soil moisture availability and atmospheric dryness on leaf phenology across tropical regions might lead to unexpected uncertainty in Earth system modelling.

5. Conclusions

This study shows that tropical trees differ greatly in canopy leaf phenology, which gradually varies from equatorial bimodal seasonality to higher-latitudes unimodal seasonality. The seasonal cycle of climate factors strongly affects that of tropical forest phenology. This study confirms that sunlight availability acts as the dominant role in controlling the seasonal leaf phenology across the pantropical forests. Importantly, our study novelty emphasizes the importance of atmospheric water stress in controlling the leaf phenology across the pantropical forests. Atmospheric dryness is always the main type of water stress in influencing the tropical leaf phenology during the first half of year. However, soil water stress separately acts as dominant water constraints on the first half of leaf phenology in tropical Asia and on the second half of leaf phenology in Congo; and shows rare impacts on leaf phenology in Amazon.

Our work contributes to a comprehensive assessment of the leaf phenology of tropical forest communities and their underlying causes. The findings of this study will be helpful to improve the authenticity and accuracy of model simulations in Earth system models. Predicting the effects of atmospheric dryness, soil water availability and sunlight availability on future tropical phenology is important for regional and global climate feedback research.

Data Availability Statement

All data used in this study are publicly available. MODIS EVI data (MYD13C2) is available at https://modis.gsfc.nasa.gov/. CSIF data is available at https://figshare.com/articles/dataset/CSIF/6387494. TWS data is available at https://figshare.com/articles/dataset/GRACE-REC_A_reconstruction_of_climate-driven_water_storage_changes_over_the_last_century/7670849. SWdown data from CRUNCEP is available at http://rda.ucar.edu/datasets/ds314.3/. ERA-Interim data used to calculate VPD is available at https://apps.ecmwf.int/datasets/.

Acknowledgments
This study was financed by the Guangdong Major Project of Basic and Applied Basic Research (grant number 2020B0301030004), National Natural Science Foundation of China (grant numbers 31971458, 41971275), Innovation Group Project of Southern Marine Science and Engineering Guangdong Laboratory (Zhuhai) (grant number 311021009) and the Special High-level Plan Project of Guangdong Province (grant number 2016TQ03Z354).

References

Araujo-Murakami, A., Doughty, C. E., Metcalfe, D. B., Silva-Espejo, J. E., Arroyo, L., Heredia, J. P., et al. (2014). The productivity, allocation and cycling of carbon in forests at the dry margin of the amazon forest in Bolivia. *Transactions - Botanical Society of Edinburgh*, *7*(1–2), 55–69.

Asner, G. P., Powell, G., Mascaro, J., Knapp, D. E., Clark, J. K., Jacobson, J., et al. (2010). High-resolution forest carbon stocks and emissions in the amazon. *Proceedings of the National Academy of Sciences of the United States of America*, *107*(38), 16738–16742.

Beer, C., Reichstein, M., Tomelleri, E., Ciais, P., Jung, M., Carvalhais, N., & Bondeau, A. (2010). Terrestrial gross carbon dioxide uptake: Global distribution and covariation with climate. *Science*. 1184984

Bhat, D. M. (1992). Phenology of tree species of tropical moist forest of Uttara Kannada district, Karnataka, India. *Journal of Biosciences*, *17*(3), 325–352.

Bradley, A. V., Gerard, F. F., Barbier, N., Weedon, G. P., Anderson, L. O., Huntingford, C., et al. (2011). Relationships between phenology, radiation and precipitation in the Amazon region. *Global Change Biology*, *17*(6), 2245–2260.

Brando, P. M., Goetz, S. J., Baccini, A., Nepstad, D. C., Beck, P. S., & Christman, M. C. (2010). *Seasonal and interannual variability of climate and vegetation indices across the Amazon*. Proceedings of the National Academy of Sciences.

Brodribb, T. J., Holbrook, N. M., & Gutierrez, M. V. (2002). Hydraulic and photosynthetic co-ordination in seasonally dry tropical forest trees. *Plant, Cell and Environment*, *25*(11), 1435–1444.

Chen, X., Ciais, P., Maignan, F., Zhang, Y., & Zhang, H. (2021). Vapor pressure deficit and sunlight explain seasonality of leaf phenology and photosynthesis across amazonian evergreen broadleaved forest. *Global Biogeochemical Cycles*, *35*(6).

Chen, X. Z., Maignan, F., Viovy, N., Bastos, A., Goll, D., Wu, J., et al. (2020). Novel representation of leaf phenology improves simulation of amazonian evergreen forest photosynthesis in a land surface model. *Journal of Advances in Modeling Earth Systems*, *12*.

Croat, T. B. (1978). *Flora of Barro Colorado island*. Stanford University Press.

Davidson, E. A., de Araújo, A. C., Artaxo, P., Balch, J. K., Brown, I. F., Bustamante, M. M. C., et al. (2012). The Amazon basin in transition. *Nature*, *481*(7381), 321–328.

De Weirdt, M., Verbeeck, H., Maignan, F., Peylin, P., Poulter, B., Bonal, D., et al. (2012). Seasonal leaf dynamics for tropical evergreen forests in a process-based global ecosystem model. *Geoscientific Model Development*, *5*(5), 1091–1108.

Descheemaeker, K., Muys, B., Nyssen, J., Poesen, J., Raes, D., Haile, M., & Deckers, J. (2006). Litter production and organic matter accumulation in exclosures of the Tigray highlands, Ethiopia. *Forest Ecology and Management*, *233*(1), 21–35.
Didan, K. (2015). MOD13C2 MODIS/terra vegetation indices monthly L3 global 0.05Deg CMG V006 [Data set]. *NASA EOSDIS LP DAAC*. https://doi.org/10.5067/MODIS/MOD13C2.006
Guan, K., Pan, M., Li, H., Wolf, A., Wu, J., Medvigy, D., et al. (2015). Photosynthetic seasonality of global tropical forests constrained by hydroclimate. *Nature Geoscience*, *8*(4), 284.
Huete, A. R., Didan, K., Shimabukuro, Y. E., Ratana, P., Saleska, S. R., Hutyra, L. R., et al. (2006). Amazon rainforests green-up with sunlight in dry season. *Geophysical Research Letters*, *33*(6), L06405.
Humphrey, V., & Gudmundsson, L. (2019). *GRACE-REC: A reconstruction of climate-driven water storage changes over the last century, Data set*, https://doi.org/10.6084/m9.figshare.7670849
Juárez, R. I. N. & Liu, W. T. (2001). Fft analysis on ndvi annual cycle and climatic regionality in northeast Brazil. *International Journal of Climatology*, *21*(14).
Kikuzawa, K. (1991). A cost-benefit analysis of leaf habit and leaf longevity of trees and their geographical pattern. *The American Naturalist*, *138*(5), 1250–1263.
Lee, J. E., & Boyce, C. K. (2010). The impact of hydraulic capacity on water and carbon cycles in tropical South America. *Journal of Geophysical Research*, *115*, D23123.
Lee, J. E., Frankenberg, C., van der Tol, C., Berry, J. A., Guanter, L., Boyce, C. K., & Badgley, G. (2013). Forest productivity and water stress in Amazonia: Observations from GOSAT chlorophyll fluorescence. *Proceedings of the Royal Society B: Biological Sciences*, *280*(1761). https://doi.org/10.1098/rspb.2013.0171
Leigh, E. G. (1999). *Tropical forest ecology: A view from Barro Colorado island*. Oxford University Press.
Lewis, S. L., Brando, P. M., Phillips, O. L., Heijden, G., & Nepstad, D. (2011). The 2010 amazon drought. *Science*, *331*(6017), 554.
Liang, X., Sassan, S. S., Yan, Y., Ranga, B. M., Christian, F., Diya, C., & Jian, B. (2015). Satellite observation of tropical forest seasonality: Spatial patterns of carbon exchange in amazonia. *Environmental Research Letters*, *10*, 084005. https://doi.org/10.1088/1748-9326/10/8/084005
Liu, L. Y., Gong, F. X., Chen, X. Z., Su, Y. X., Fan, L., Wu, S. B., et al. (2021). Bidirectional drought-related canopy dynamics across pantropical forests: A satellite-based statistical analysis. *Remote Sensing in Ecology and Conservation*. https://doi.org/10.1002/rse2.229
Liu, L. Y., Liao, J. S., Chen, X. Z., Zhou, G. Y., Su, Y. X., Xiang, Z. Y., et al. (2017). The Microwave Temperature Vegetation Drought Index (MTVDI) based on AMSR-E brightness temperatures for long-term drought assessment across China (2003–2010). *Remote Sensing of Environment*, *199*, 302–320. https://doi.org/10.1016/j.rse.2017.07.012
Lopes, A. P., Nelson, B. W., Wu, J., Mauricio, P., Tavares, J. V., Prohaska, N., et al. (2016). Leaf flush drives dry season green-up of the Central Amazon. *Remote Sensing of Environment*, *182*, 90–98.
Luo, Y. X., Ma, J., & Zhu, Q. S. (2003). Matlab-based signal phase difference of mutual function method. *Science and Technology Information Development & Economy*, *13*(7), 149–150.
Malhado, A., Costa, M. H., Lima, F., Portilho, K. C., & Figueiredo, D. N. (2009). Seasonal leaf dynamics in an amazonian tropical forest. *Forest Ecology and Management*, *258*(7), 1161–1165.
Malhi, Y., Adu-Bredu, Asare, R. A., Lewis, S. L., et al. (2013). African rainforests: Past, present and future. *Philosophical Transaction of Royal Society B*. (1625), 368. https://doi.org/10.1098/rstb.2012.0312
Malhi, Y., Nobre, A. D., Grace, J., Kruijt, B., Pereira, M., Culf, A., & Scott, S. (1998). Carbon dioxide transfer over a central amazonian rain forest. *Journal of Geophysical Research*, *103*(D24), 31593–31612. https://doi.org/10.1029/98JD02647
Moraes, R., Delitti, W. B. C., & Struffaldi, D. Y. (1999). Litterfall and litter nutrient content in two Brazilian Tropical Forests. *Brazilian Journal of Botany*, *22*(1), 09–16.
Morton, D. C., Nagol, J., Carabajal, C. C., Rosette, J., Palace, M., Cook, B. D., et al. (2014). Amazon forests maintain consistent canopy structure and greenness during the dry season. *Nature*, *506*(7487), 221.
Oguntunde, P. G. (2005). Whole-plant water use and canopy conductance of cassava under limited available soil water and varying evaporative demand. *Plant & Soil*, *278*(1-2), 371-383.
Restrepo-Coupe, N., da Rocha, H. R., Hutyra, L. R., da Araujo, A. C., Borma, L. S., Christoffersen, B., et al. (2013). What drives the seasonality of photosynthesis across the Amazon basin? A cross-site analysis of eddy flux tower measurements from the Brazil flux network. *Agricultural and Forest Meteorology*, *182*, 128–144.
Saleska, S., Rocha, H. D., Kruijt, B., & Nobre, A. (2009). Ecosystem carbon fluxes and amazonian forest metabolism. *Geophysical Monograph Series*, *186*, 389–407.
Shaw (2016). Rainfall, leafing phenology and sunrise time as potential Zeitgeber for the bimodal, dry season laying pattern of an African rain forest tit (Parus Fasciiventer). *Journal of Ornithology*, *158*(1), 263–275. https://doi.org/10.1007/s10336-016-1395-6
Sulla-Menashe, D., Woodcock, C. E., & Friedl, M. A. (2018). Canadian boreal forest greening and browning trends: An analysis of biogeographic patterns and the relative roles of disturbance versus climate drivers. *Environmental Research Letters*, *13*(1), 014007.
Taiz, L., & Zeiger, E. (2002). *Plant physiology* (3rd ed., pp. 423–459). Sinauer Associates.
Tang, H., & Dubayah, R. (2017). Light-driven growth in Amazon evergreen forests explained by seasonal variations of vertical canopy structure. *Proceedings of the National Academy of Sciences*, *114*(10), 2640–2644.
Viovy, N. (2018). *CRUNCEP version 7 - Atmospheric forcing data for the community land model*. Research Data Archive at the National Center for Atmospheric Research, Computational and Information Systems Laboratory.
Vourlitis, G. L., José, D. S. N., Filho, N. P., Hoeger, W., Raiter, F., Biudes, M. S., et al. (2005). The sensitivity of diel CO_2 and H_2O vapor exchange of a tropical transitional forest to seasonal variation in meteorology and water availability. *Earth Interactions*, *9*(27), 1–23.
Wang, Z. X., Liu, C., & Huete, A. (2003). From avhrr-ndvi to modis-evi: Advances in vegetation index research. *Acta Ecologica Sinica*, *23*(5), 979–987.
Wiener, N. (1988). The fourier integral and certain of its applications: Plancherel's theorem. *Nature*, *132*(3341), 731–732.
Wright, S. J., Carel, P., & Schaik, V. (1994). Light and the phenology of tropical trees. *The American Naturalist*, *143*(1).
Wu, J., Albert, L. P., Lopes, A. P., Restrepo-Coupe, N., Hayek, M., Wiedemann, K. T., et al. (2016). Leaf development and demography explain photosynthetic seasonality in Amazon evergreen forests. *Science*, *351*(6276), 972–976.
Xiao, X., Hagen, S., Zhang, Q., Keller, M., & Moore, B. (2006). Detecting leaf phenology of seasonally moist tropical forests in South America with multi-temporal modis images. *Remote Sensing of Environment*, *103*(4), 465–473.
Yang, X. Q., Wu, J. P., Chen, X. Z., Ciais, P., Maignan, F., Yuan, W. P., et al. (2021). A comprehensive framework for seasonal controls of leaf abscission and productivity in evergreen, broadleaved tropical and subtropical forests. *The Innovation*, 100154. https://doi.org/10.1016/j.xinn.2021.100154

Yuan, W., Zheng, Y., Piao, S., Ciais, P., Lombardozzi, D., Wang, Y., et al. (2019). Increased atmospheric vapor pressure deficit reduces global vegetation growth. *Science Advances*, *5*(8), eaax1396.

Zeng, Y., Badgley, G., Dechant, B., Ryu, Y., Chen, M., & Berry, J. A. (2019). A practical approach for estimating the escape ratio of near-infrared solar-induced chlorophyll fluorescence. *Remote Sensing of Environment*, *232*, 111209.

Zhang, H., Yuan, W., Dong, W., & Liu, S. (2014). Seasonal patterns of litterfall in forest ecosystem worldwide. *Ecological Complexity*, *20*, 240–247.

Zhang, Y., Joiner, J., Alemohammad, S. H., Zhou, S., & Gentine, P. (2018). A global spatially contiguous solar-induced fluorescence (CSIF) data set using neural networks. *Biogeosciences*, *15*(19). https://doi.org/10.5194/bg-15-5779-2018

Zheng, P. G., Liu, Z. X. (1986). The definition and calculation of partial correlation coefficient. *Journal of Jiangxi University of Finance and Economi*, (01), 79-83.

Zhou, S., Zhang, Y., Williams, A. P., & Gentine, P. (2019). Projected increases in intensity, frequency, and terrestrial carbon costs of compound drought and aridity events. *Science advances*, *5*(1), eaau5740. https://doi.org/10.1126/sciadv.aau5740